Applied Clay Science 178 (2019) 105126

Contents lists available at ScienceDirect

Applied Clay Science

journal homepage: www.elsevier.com/locate/clay

Research paper

α-Cristobalite formation in ceramic tile and sewage pipe bodies derived from Westerwald ball clay and its effect on elastic-properties

Aydın Aras[a,*], Ferenc Kristaly[b]

[a] Yuzuncu Yıl University, Engineering and Architecture Faculty Geological Engineering Department, 0 6580 Van, Turkey
[b] Department of Mineralogy and Petrology, University of Miskolc, 3515 Miskolc-Egyetemváros, Hungary

ARTICLE INFO

Keywords:
X-ray diffraction
High-temperature phases
Ceramic
α-cristobalite
Elastic modulus

ABSTRACT

The formation of α-cristobalite and its effect on the elastic modulus (E modulus) was investigated in sewage pipe (SP) and tile bodies derived from Westerwald ball clay (WBC), employing the results of previous research on WBC as a baseline. In this study, the SP and tile bodies derived from WBC are compared with the bodies derived from two residual Turkish kaolin and one Turkish ball clay, resulting in four sources of α-cristobalite formation: tile, SP, residual kaolin and ball clay. The crystallization of α-cristobalite in the fired WBC results from two primary pathways. The first pathway occurs as a devitrification product from the glass phase saturated with excess silica, which is typically present in ball clay after ≥1100 °C; the second pathway results from a minor amount of transformation of peripheries of quartz crystals, firing at over ≥1200°. In addition to these two sources, other α-cristobalite sources for sewage-pipe bodies include smectitic clay and chamotte (prefired clay) addition. Conversely, no α-cristobalite occurred in tile mixture bodies containing ≈2 wt% potassium oxide (K_2O). The α-cristobalite phase only forms in kaolinite-rich ball clay when K_2O content is less than ≈2 wt% because devitrification of excess silica phase of tile bodies is primarily governed by K_2O content. The ≈2 wt% K_2O ratio inhibited α-cristobalite formation in tile bodies, while the same percentage or greater of K_2O content in SP bodies did not inhibit the α-cristobalite formation due to the presence of chamotte and smectitic clay in the SP mixture. The measured minimum E moduli were attributed to cristobalite formations because of chamotte and smectitic clay additions to SP bodies. In the bodies derived from Turkish residual kaolin at over 1000 °C, the opaline and chalcedonic silica phase are transformed to α-cristobalite at a lower temperature than those observed for rock crystal quartz and Si-rich glassy phase in WBC bodies. Thus, determining the different α-cristobalite sources in clay-based ceramic bodies derived from either the ball clay, the residual kaolin or the bodies containing smectitic clay together with chamotte provides the essential pre-condition for the optimum admixing ratio in industrial SP and tile bodies.

1. Introduction

The physical and mechanical properties of clay-based ceramic bodies derived from Westerwald ball clay or kaolinite are affected by the mineral phases formed during the firing process, which we refer to in this study as newly formed phases. These newly formed minerals include silicates such as mullite minerals that are beneficial to the physical and mechanical properties of the ceramic bodies (Carty and Senapati 1998; Barbieri et al., 1995). When kaolinitic clays are used for clay-based ceramic products, the presence of mullite in the bodies denotes a well-fired body. Mullite is a hard, chemical-resistant phase, and its elongated crystal structure provides great strength (Carty and Senapati 1998; Cavalcante et al., 2004; Zanelli et al., 2011). However, the newly formed minerals also include oxides such as cristobalite (e.g., SiO_2, CaO or FeO), which.

lower the quality of the product. Because, the newly-formed cristobalite together with residual quartz negatively influence the strength of ceramic bodies due to the large volume change (1 wt%) of α-β inversion of quartz at 573 °C and volume change (2.8 wt%) of α-β inversion cristobalite at 220 °C (Iqbal and Lee, 1999). As a result, large stresses may arise as a result of the in-mismatch expansion between these minerals and Si-rich glassy phase. The low strength level is attributable mainly to the presence of this large internal stresses, which often results in microcracks and flaws within the quartz and cristobalite grains and around these minerals peripheries and through the glassy matrix (Stubna et al., 2007). Therefore, the newly-formed α-cristobalite negatively influences the physical properties of a clay-based ceramic body, such as thermal expansion, flexural strength, and thermal shock

* Corresponding author.
E-mail address: aras5549@yahoo.com (A. Aras).

https://doi.org/10.1016/j.clay.2019.105126
Received 1 April 2019; Received in revised form 4 May 2019; Accepted 9 May 2019
Available online 31 May 2019
0169-1317/

resistance. On the other hand, numerous studies have been made on the newly formed mullite occurrences from kaolinitic clays suchs as kaolin (Gualtieri et al. 1995) ball clay (Herrera et al., 2019) and allophane (Du et al., 2018). One such newly formed phase, even if less studied in this context, is cristobalite, the most common α (low-temperature) form that is also preserved during cooling based on X-ray diffraction and SEM studies (Lundin 1964). The type, amount and size distribution of newly formed mullite and α-cristobalite in these ceramic bodies are primarily governed by three factors: a) the alkaline and alkaline-earth non-clay and clay impurities (Johnson and Pask, 1982), b) the type, amount and size distribution of silica phase (Wahl et al., 1961), and c) the crystallinity degree of kaolinite minerals (Dubois et al., 1995; Gualtieri et al., 1995). The appearance and disappearance of both mullite and α-cristobalite in the amorphous/glassy phase depend on those above three basic properties, which are closely correlated to each other. The main constituents of these ceramic bodies made of kaolinitic clay are potassium-rich minerals, illite and sericite variety of serisitic mica, and feldspars beyond kaolinite and ball clay. However, the differing geological deposition environment of kaolinitic clays leads to variations in kaolinite-crystallinity. The deposits are formed from granitic and micaceous rocks and are either deposited in-situ and called residual clay (i.e., kaolin) or are transported and deposited in sedimentary clay (i.e., ball clay). Three important differences are present between ball clay and residual kaolin. The first difference is that ball clay is more highly variable in mineralogical composition than residual clay, and the most common fine-sized impurities are macrocrystalline rock crystal quartz, illite, smectite, and feldspar, which are found mixed with disordered kaolinite in sedimentary processes (Wilson, 1998; Mitchell and Vincent, 1997). In residual clays, these minerals are generally present as much coarser grains and can be easily separated apart from microcrystalline silica (i.e., chalcedony) or opaline silica through beneficiation with the washing-settlement process. The second difference is the degree of crystallinity of kaolinite minerals: these minerals are poorly crystallized in ball clay and are well and highly crystallized when found in residual kaolin and show different firing behavior (Glass, 1954; Wahl et al., 1961; Onike and Martin, 1986; Johnson and Pask, 1982; Gualtieri et al. 1995; Zhou et al., 2013; Dubois et al., 1995). The third difference is the type of silica phase: in general, rock crystal quartz is present in ball clay, whereas, in hydrothermal kaolin, the silica phases occur as opaline and chalcedonic. In preparation of ceramic bodies in this investigation, we used fine-grained, highly plastic and mainly kaolinitic sedimentary clay of Westerwald area classified as “ball clay” (Wilson, 1998; Mitchell and Vincent, 1997; Chmelik et al., 2011) and two hydrothermal-residual clays: The Turkish clays DM and KU with medium crystallinity containing chalcedony and opal-CT (Fuji et al., 1980; Fuji et al., 1995; Okut and Gok, 1975) and Turkish ball clay are used to compare with WBC. Thus, the pathways of α-cristobalite formation of three possible sources; a) individual kaolinitic WBC, b) their mixture used in tile and SP production, and c) individual residual Turkish kaolin were investigated based on the results of a former study by Aras (2004), Aras et al. (2007) and Aras (2018) in this study. All these fired experimental ceramic bodies (three axial bodies: Clay + Feldspar + Quartz) consist mostly of mullite, α-cristobalite and Si-rich glassy phase after firing (Martin –Marquez et al., 2008). Due to the relatively important Na and K content of kaolinitic clay which has illitic and smectitic clay impurities, K or Na feldspar and their associated phases, these products are also known as alkaline bodies, besides all commercial bodies should be considered as alkaline bodies because the feldspar minerals which should be in their receipts.

On the other hand, it is generally known that the strength and elastic constant of clay-based ceramic bodies decrease with an increasing amount and size of porosity and quartz grain (Warshaw and Seider, 1967; Pickup, 1997). However, in the present study, in SP bodies, the 10 wt% smectite and 20 wt% chamotte additions should be used for providing of dimensional stability and to increase of dry strength because of the large shaped green SP body mixture, but unfortunately these additions caused additional cristobalite formation that creates increasing porosity and decreasing in elastic modulus. Garg and Skibsted. (2014) reported that cristobalite was identified in aluminosilicate of calcined smectitic clay, i.e., montmorillonite at above 950 °C. Trümer et al. (2019) stated that also crypto crystals as described by Garg and Skibsted (2014), i.e., cristobalite was identified in calcined smectitic clay of Westerwald at 900 °C. This slightly lower temperature 900 °C gave better result on pozzolanic properties of heated Westerwald clay (Trümer et al., 2019). The low amount of inert cristobalite formation at low temperature may be reason of this better result. Therefore the primary aim of this study is to investigate and determine the possible pathways, and sources of cristobalite formation in an alkaline ceramic body derived from individual residual kaolin and ball clay or tile and SP body mixtures containing both type of clays, feldspar, chamotte and smectitic clay and their effects on E modulus.

2. Materials and method

2.1. Mineralogical properties of WBC

In general, the WBC are natural mixtures of fine particle-sized, disordered kaolinite, typically mixed with mica/illite, feldspars, quartz, a small amount of smectite, and other oxide minerals. These ball clays yield a high strength, plastic, light burning clay, which is particularly suited to the ceramic tile and stoneware (Kromer, 1968–1979; Kromer, 1980; Fiederling-Kapteinat, 2005). In a previous study, three WBC were selected and investigated by (Aras et al., 2007; Aras 2004; Aras, 2018). These clays are representative of the high kaolinitic (HB), illitic (KW) and naturally mixed kaolinite-illite (P1) clay of Westerwald. In the previous work, these extreme compositions were chosen because all WBC used for tile and SP production are of these types or intermediate between them. The results from the chemical and mineralogical analysis of extreme compositions of WBC; HB, KW, and P1 of previous studies, and their mixtures are given Table 1 and Table 2.

The intermediate compositions of three tile clays (432, 295 and 394) and five SP clays (MG8048, TK 8048, MG 8214, T2105 and MRM)

Table 1
Mineralogical composition of the previous study of WBC (Aras, 2018).

WBC	Kaolinite	Illite	I/S mix lay.	Na-Ca felds	K felds	Quartz tros-wyn	Fe, Ti minerals
HB	72(77)	13(12)*	3	–	1	8(4.5)	2
75wt%HB + 25wt%KW	58	17	2	2	–	18	1
50wt%HB + 50wt%KW	40	21	1	4	–	31	1
25wt%HB + 75wt%KW	24	25	–	6	–	42	–
KW	7(14)	21(30)	–	8	–	55(53)	–
P1	41(31)	32(44)	2	1	2	20(24)	1
Turkish clays*							
ŞE-2	24.0	2	1	–	1	67(Rock Qua)	–
DM	45,6	–	(2)Smec 14A	–	–	52 (Chalcedon)	–
KU	53,6	–	(2)Tri-Oc Smec	–	–	45(Op-CT) + Q	–

–not determined () Calculated data *Literature data: (Okut and Gok, 1975; Fuji et al., 1980.

Table 2
Chemical composition of the previous study of WBC (Aras 2004).

WBC	SiO_2	Al_2O_3	Feo	MnO	MgO	CaO	Na_2O	K_2O	TiO_2	P_2O_5	LO I	Total
HB	45.60	37.76	1.66	0.01	0.49	0.56	0.18	0.91	2.48	0.04	12.59	99.28
75 wt%HB + 25 wt%KW	52.40	32.35	1.45	0.01	0.46	0.50	0.28	1.3	2.10	0.04	10.3	99.26
50 wt%HB + 50wt%KW	59.30	26.30	1.26	0.01	0.40	0.40	0.40	2.02	1.72	0.05	7.95	99.25
25wt%HB + 75wt%KW	66.20	21.49	1.06	0.01	0.40	0.38	0.50	2.53	1.34	0.05	5.90	99.54
KW	73.07	6.12	0.87	0.01	0.43	0.33	0.62	3.61	0.97	0.06	3.66	99.22
P1	56.8	28.8	0.93	0.01	0.61	0.28	0.13	3.58	1.1	0.04	7.96	99.26
Turkish clay[a]												
ŞE-2	75.8	14.0	1.7	1.02	0.1	0.2	0.1	1.5	1.2	0.1	4.05	99.80
KU	67.0	21.5	0.3	1.0	1.0	0.2	1.0	0.4	0.1	0.2	8.40	99.94
DM	71.5	20.3	0.4	0.1	0.2	0.1	0.1	0.1	0.4	0.1	6.1	99.50

[a] Literature data: (Okut and Gok, 1975; Fuji et al., 1980).

Table 3
Mineralogical composition of the tile and SP clays of Westerwald and Turkish ball and residual clays and tile and SP body mixtures.

WBC	Kaolinite	Illite	I/S mix lay.	Na-Ca felds	K felds	Quartz tros-wyn	Fe, Ti minerals
Tile clays							
295	35(30)	18	–	2	2	43(45)	–
394	43(40)	20	–	–	–	30(33)	–
432	70(70)	12	–		–	18(20)	1
TMIX*	40	12	–	2	–	45	–
TMIXK	30	8	–	–		43	–
TMIXC	32	8	–	–		44	–
SP clays							
MG-8048	23	20	10	2	–	46	2
TK-8048	23	20	10	2	–	49	2
MG-8214	18	18	9	2-		54	1
T-2105	40	20	10	2	–	18	3
MRM	45	18	12	2	–	12	8
SPMIX**	24	19	10	2	–	44	3

–not determined.
() Calculated data.
** SPMix:40 wt % MG8214 + 40 wt TK 8048(or MG 8048) + 10 wt % T2105 + 10 wt % MRM.

were selected for this work. The X-Ray analysis shows that the studied tile and SP clays of Westerwald area mainly consist of kaolinite, illite and quartz and minor amounts of anatase, feldspar, and mixed layered illite/smectite. The results from the chemical and mineralogical analysis of the studied selected clays are given in Tables 3 and 4. Therefore, the studied clays can also be called "kaolinite-illite-quartz" clays. Semi-quantitative estimations of kaolinite and illite in the < 2 μm fraction were made from the (001) lines. Areas under the peaks were measured in preference to peak heights and illite was used as an internal standard while the regions of the kaolinite peaks were divided by 3 (Biscaye, 1965; Vandenberghe, 1978). Moreover, then, all measured values so obtained were normalized to wt%100. The combination of X-ray diffraction and chemical analysis yields reliable quantitative information on the mineral composition of these selected clays because they have simple mineralogical compositions, primarily consisting of kaolinite, illite, and quartz, but the free quartz content is also determined by Trostel and Wynne (1940) method and as shown in Table 3. Therefore the semi-quantification of the mineralogical composition using X-ray patterns and calculated mineralogy from chemical analysis correspond very well.

The X-ray analysis reveals that the studied WBC mainly consist of illite, kaolinite and quartz and other very small amounts of minor constituents such as anatase and feldspar except for MRM containing smectitic clays as mentioned earlier. According to the extreme compositions of HB and KW, as mentioned previously in Tables 1, 2, the studied tile and SP clays mineralogically represent some composition between them (Table 3, 4). The high SiO_2 concentration always correlates with high quartz content. The quartz is mostly in the form of fine or very fine-grained sand and silt spread through the particle size distribution (SEM studies). The CaO and MgO content are always low, and the higher K_2O content usually correlates with the mica minerals, sericitic mica /illite, but also with the small portion of potassium feldspar (Table 4). The K_2O has been determined as the important primary composition that inhibits the formation of cristobalite in tile and SP

Table 4
The chemical composition of tile and SP clays of Westerwald and Turkish ball and residual clays and tile and SP body mixtures.

BC	SiO_2	Al_2O_3	Feo	MnO	MgO	CaO	Na_2O	K_2O	TiO_2	P_2O_5	LO I	Total
Tile clays												
295	66.06	21.6	1.23	0.01	0.42	0.19	0.17	2.47	1.23	0.07	5.93	99.38
394	61.94	24.27	1.04	0.01	0.39	0.25	0.16	1.93	1.72	0.06	7.28	99.48
432	54.19	29.90	1.6	0.01	0.75	0.25	0.14	0.74	1.46	0.04	10.38	99.46
TMIX	60.18	25.69	1.44	0.01	0.58	0.43	0.14	1.71	1.46	0.08	7.73	99.36
TMIXC	59.71	25.42	1.19	0.01	0.53	1.60	1.39	1.52	1.25	0.07	6.62	99.31
TMIXK	58.82	26.12	1.21	0.01	0.53	0.53	0.58	2.96	1.23	0.07	6.56	99.21
SP clays												
MG-8048	68.73	18.76.	2.25	0.01	0.42	0.29	0.17	2.47	1.24	0.07	5.93	99.10
TK-8048	71.01	16.95	2.21	0.01	0.34	0.19	0.19	2.06	0.95	0.06	5.01	99.25
MG-8214	74.5	15.70	1.5	0.01	0.31	0.16	0.09	1.79	0.86	0.04	5.01	99.40
T-2105	52.4	25.20	3.37	0.01	0.49	0.22	0.15	2.21	1.05	0.05	5.80	99.36
MRM	66.2	26.80	8.32	0.01	0.92	0.51	0.08	2.08	1.25	0.08	5.60	99.35
SP Mix	70.56	21.45	2.18	0.01	0.56	0.32	0.13	1.96	1.56	0.08	5.36	99.56
SP Mix-Cham T	72.3	19.8	2.33	0.01	0.48	0.25	0.12	1.53	1.21	0.08	4.42	99.33

TMIX: 30 wt% 295 + 40 wt% 39 + 30 wt% 432. TMIXK: 25 wt% 295 + 30 wt% 394 + 25 wt% 432 + 20 wt% K felds.
TMIXC: 25 wt% 295 + 30 wt% 394 + 25 wt% 432 + 20 wt% Ca−Na felds.
SP Mix: 40 wt% MG 8214 + wt% 40 T 8048(or MG8048) + 10 wt% T 2105 + 10 wt% MRM.
SP Mix-Chamotte: 80 wt% SP Mix + 10 wt% MRM or T2105 or TK 80 + 20 wt% Chamotte.

bodies. The cristobalite can be formed when a content of K_2O is lower than > 2 wt% in the bodies derived from individual WBC and its Ca−Na feldspar mixture. No cristobalite formed in the ceramic bodies derived from illitic KW and HK and P1 containing ≥ 2 wt% K_2O (Tables 1, 2). Further form, in these bodies containing ≥ 2 wt% K_2O, also no spinel is formed. Slaughter and Keller (1959) reported that no spinel phase occurs as an intermediate phase in flint clay containing ≥ 2 wt% K_2O.

2.2. Mineralogical properties of residual Turkish kaolin

The two residual Turkish clays (DM and KU), formed by hydrothermal alteration of tuffaceous rocks, and one Turkish ball clay (ŞE) from the Şile area were selected and compared with WBC. For more detailed geological and mineralogical information of Turkish clays, refer to the studies of Aras et al. (2007), Okut et al. (1978), Fuji et al. (1980), Fuji et al., 1995and Ece et al. (2003). These clays have different firing responses as a result of different geological origin, clay mineral crystallinity and chemical purity. The DM and KU clays were also investigated for the cement and concrete industry (Aras et al., 2007). The DM clay is the hydrothermal alteration of tuffaceous sandstone and thus contains chalcedonic aggregates (Okut and Gok, 1975). The KU clay is a hydrothermal alteration of dacitic tuff and includes opaline silica (Fuji et al., 1980). Table 1 summarizes the composition of the investigated clays as primarily consisting of quartz, chalcedony, opal-CT, and kaolinite with medium crystallinity as defined by Hinckley index (Guggenheim et al., 2001-2002) and both of them cause of low plasticity. The Şile clay (ŞC) is plastic sedimentary ball clay, also containing a significant amount of rock crystal quartz (Ece et al., 2003) (Table 3 and Table 4).

2.3. Crystallization degree of tile and SP clays

For WBC with an increasing structural disorder on the b-axis and decreasing grain size, the plasticity improves and such intermediate stages are referred to as structurally disordered kaolinite or fireclay (Kromer, 1968–1979) (Guggenheim et al., 2001-2002). WBC are similar in basic mineralogical composition to fireclay. As a result, the temperature over which WBC begins to fuse partially, therefore, the WBC's firing behavior is characterized by a relatively wide reaction, and the same broad reaction is observed for Al-rich fire clays. The X-ray pattern of these clays also reveals a more significant sequence disorder. If the X-ray pattern of Turkish residual kaolin compared with those of Westerwald and Turkish ball clays. The X-ray patterns of all the studied ball clay display fewer reflections and resemble those of fireclay (i.e., flint clay or underclay) (Keller, 1968; Chavez and Johns, 1995) (Fig. 1). Because the characteristic triplets of well-crystallized kaolin are primarily replaced by doublets of ball clay and the basal reflections are both less sharp and less intense than those of residual kaolin (Thorez, 1976) (Fig. 1).

2.4. Preparation of the tile and SP bodies

The complete characterization results of the extreme composition of WBC is reported in detail in Aras (2004) and Aras (2018) (Table 1) (Table 2). The intermediate compositions of Westerwald ball clays and K and Ca−Na feldspar selected for this study are; three tile clays (432-Ton GF), 295 (Fuchs'sche Tongruben) and 394 (Stephan-Schmidt KG) and five SP clays (MG8048, TK 8048, MG 8214, T2105 and MRM) (Steinzeug-Keramo N·V). Ca−Na Feldspar Labradorite-Bytownite. HSN H.J.Schmıdt K.G Helvik-Split), K feldspar (Baux Feldsspaths ST-Paul-De Fennouillet). The tile bodies were derived from individual and tile clay mixtures (TMIX) and 80 wt% TMIX + 20 wt% K-feldspar and Ca−Na Feldspar (TMIXK and TMIXC). The SP bodies derived from individual SP clays and SP Mıx of SP clays and 80wt%SP Mıx + 20 wt% Chamotte and 10 wt% MRM or T2105 or TK8048. The full body formulas are given in Table 3 and Table 4. Due to the need for a continued production rate of tile and SP at the same level and the necessity to comprise mixtures of these selected clays up to 3 or 5 different types of clay of Westerwald region were mixed.

2.5. X-ray diffraction analysis of the fired bodies

The interrupted-quench samples X-ray analysis (QSXRD) could represent a powerful tool to improve the identification and development of mullite and α-cristobalite. The tile and SP mixtures undergo mineralogical changes depending mainly on the type and amount of mineral impurities found in these clays and non-clay and on the heat treatment parameters. For this study the heat treatment parameters of heating rate, soaking time (dwelling time) and firing-atmosphere are fixed at 2 °C/min, 2 h and oxidizing atmosphere respectively. The reference card numbers and the relative intensities for the major and minor phases' strongest reflections have been obtained from the ICDD database. Identification can be confirmed through comparison with the complete diffraction pattern provided on ICDD database with Panalytical.-High-Score software. The major intense reflections from these minerals are restricted within the narrow 20–40° 2θ angle range. Since all of these minerals are frequently present this narrow-angle range leads to overlapping reflections and non-measurable reflections from less abundant mineral components. An example of the difficulties encountered is when hematite or anorthtite is identified in the presence of α-cristobalite. The studied clay-based ceramic bodies exhibit a phase composition made of a glassy phase, residual quartz and feldspar (most of them melt) and newly formed mullite and cristobalite. Here is the important crystalline phase residual quartz and mullite and their quantities are well observed with pair reflections of 1.54 Å (Q)-1, 52 Å (M) at 2Θ (60.02–60.81) or 1.84 Å (M)–1.82 Å (Q) at 2 Θ (49.54–50.19). Thus, the change of relative intensities of these reflection pairs; indicates the relative abundance of mullite and residual quartz in the fired body or kaolinite and quartz ratio in green bodies.

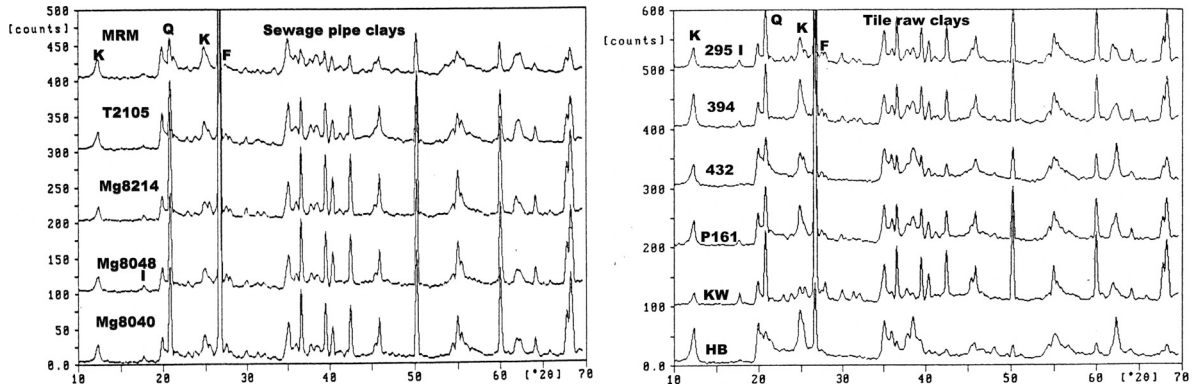

Fig. 1. X-ray diffraction patterns of the individual raw tile and SP clays (K: Kaolinite. Q: Quartz. F: Feldspar and I: Illite).

2.6. Chemical analysis

The mineralogical and chemical composition of these WBC and their mixtures prepared for tile and SP production are given in Table 1 and Table 2. Chemical analyses were obtained by optical emission spectrometry with an inductively coupled plasma (ICP-OES) source and an atomic emission source (ICP-AES) for major elements after fusion with $LiBO_2$ and dissolution in HNO_3. For sampling criteria and procedures as well as methodologies followed in mineralogical. Chemical, granulometric and physical properties of green and fired bodies refer to Aras (2004) and Aras et al. (2007).

2.7. Scanning electron microscopy (SEM)

The SEM micrographs were taken from a fractured surface of tile and SP bodies fired at 1200 °C The fractured fresh surfaces were treated during 1, 2, or 3 min with hot and cold HF. SEM observations were made on fresh broken or etched-fresh broken surfaces of tile and SP bodies after coating with gold. The crystals were examined at 20–30 kV accelerating voltage with a Jeol JSM 6400 equipped with a Link energy dispersive spectrometer for qualitative analysis. The reflection heights for the same element of the different spectrum are used as a measure of the individual element concentration.

2.8. Measurement of density, porosity and E modulus of tile and SP bodies

2.8.1. Porosity and density

There are three volume expressions in the measurements of density and porosity of the fired tile and SP bodies by using “Accupyc 1330” pycnometer. First one; a)-Apparent volume (direct measurements of perfect shape). It is an “envelope” volume of the fired product sometimes referred to as the “bulk volume” and includes the volume of the solid components, open pores, and closed pores. Second; b)-Real volume (Accupyc-1330) refers to the volume of just the solid components of the fired bodies. It was determined by crushing the fired body into powder by using a vibratory mill for half an hour so that all the pores are destroyed. Third; c)-Skeletal volume (Accupyc1330). This volume lies between (a) and (b), it is the volume of solid components and closed pores only. Consequently, there are three expressions of density corresponding to the three-volume expressions defined above.

a) - Apparent density (bulk density) b) - Real density c) - Skeletal density.

Apparent density is calculated from the volume of perfect shape and the weight during measurement of elastic modulus. Skeletal and real density measurements were made using the Accupyc-1330 pycnometer. Skeletal density is measured from undestroyed pieces of a fired body but real density measured from the powder of fired body. The instruments increase the precision of the analysis result by reporting data from several consecutive runs (one complete measurement) and calculating average volume density and standard deviations. Three types of porosity related to the densities calculated and expressed as a percentage are the following.

$$App\ por\ wt\% = 100\frac{1 - App.\ Den}{Ske.\ den},\ True\ por\ wt\%$$
$$= 100\frac{1 - App\ den}{Real\ den},\ Closed\ por\ wt\%$$
$$= 100\ x\ App\ den\frac{1 - App\ den}{Ske\ den} - \frac{1}{Real\ den}$$

It is known that apparent porosity is often given in the form of water absorption. The determination of water absorption is commonly used because it is simple and less time consuming than the measurement of apparent porosity.

2.9. Elastic modulus (E modulus)

A grindosonic instrument-MK-5 was used to determine the dynamic E modulus and utilizes the principle that elasticity theory can be applied to fired tile and SP bodies (Lemmens,1990). The instrument directly measures the fundamental vibration frequency in a ceramic body of regular shape dimensions following shock excitation. Ceramic materials possess specific mechanical resonance frequencies which are defined by the elasticity, density, and geometry of the test specimen. Therefore, the elastic properties of a material can be computed if the geometry, density and mechanical resonance frequencies of suitable test specimens of ceramic material can be measured. E modulus is determined using the resonance frequency in the flexural mode of vibration. The sample is struck to set up a mechanical vibration pattern rather than being subjected to continuous flexure. This pattern is converted to an electronic signal via a piezo-electric detector held in contact with the test piece surface. The apparatus amplifies the signal. If it exceeds the predetermined minimum level required for analysis, the time of eight wave passes is measured. A short interval between striking the sample and measurement prevents the analysis of spurious initial wave patterns which have complex harmonics and which occur when the test piece is initially struck. The elapsed time appears as a result of the equipment display panel and is known as the -r- value (reading). The “r” value, the dimensions and the mass of the specimen are fed to the computer for calculation of E modulus using the following formula

$$Eflex\frac{m}{br^2}[(l/h)^3 * C1 + (l/h) * C2]$$

where m = Weight, l = Length, b = Width h = thickness r = grindosonic reading E = E modulus kN/mm^2 or GPa, C_1, and C_2 = two constants.

Test samples to be used with the ultrasonic apparatus can be cut to a variety of shapes including bars cylinders and discs. There are however nominal limits for sample dimensions, for this study bar-shaped were pressed fired and used for these measurements. These must have a length to thickness ratio of more than three and the width of the bar should be less than one-third of the length. Beyond these limits, the calculation gradually loses accuracy. For the precision of the analysis result by reporting data from 5 consecutive runs (one complete measurement) and calculating average E modulus and standard deviations. A variation of < 0.5 wt% in several successive measurements of the same body is typical when measuring tile and SP bodies, after a few minutes of practice grindosonic readings (resonant frequency) can be obtained with a standard deviation approaching zero.

3. Results

3.1. QSXRD X-ray diffraction patterns of tile bodies derived from individual tile clay 295. 394 and 432 and their mixtures (TMIX) mixed with 20 wt% K or Ca–Na feldspar (Fig. 2)

The only mineral phases present at 1150 °C. 1175 °C and 1200 °C were quartz and mullite in the bodies of 295 and 394. The newly-formed mullite reflection intensities slightly increase with increasing temperature, while the quartz reflection intensities remain the same. No α-cristobalite was detected in 295 and 394 bodies containing 20 wt% K and Ca–Na bodies. K feldspar completely melted at 1200 °C but there was only a slight decrease in Ca–Na feldspar, and their reflections remained at 1200 °C. After the addition of K- and Ca–Na feldspar a decrease in the intensities of mullite and quartz reflections was observed. The high potassium content of samples 295 and 394 originated from illitic clay, and K feldspar impurities of these clays inhibit α-cristobalite formations (Fig. 1). The appearance of 1.60 Å, 2.08 Å and 2.38 Å were due to the contamination of sample powder of fired bodies of 432, 295 and 394 in grinding in corundum cell.

At temperatures of 1150 °C. 1175 °C and 1200 °C the only mineral

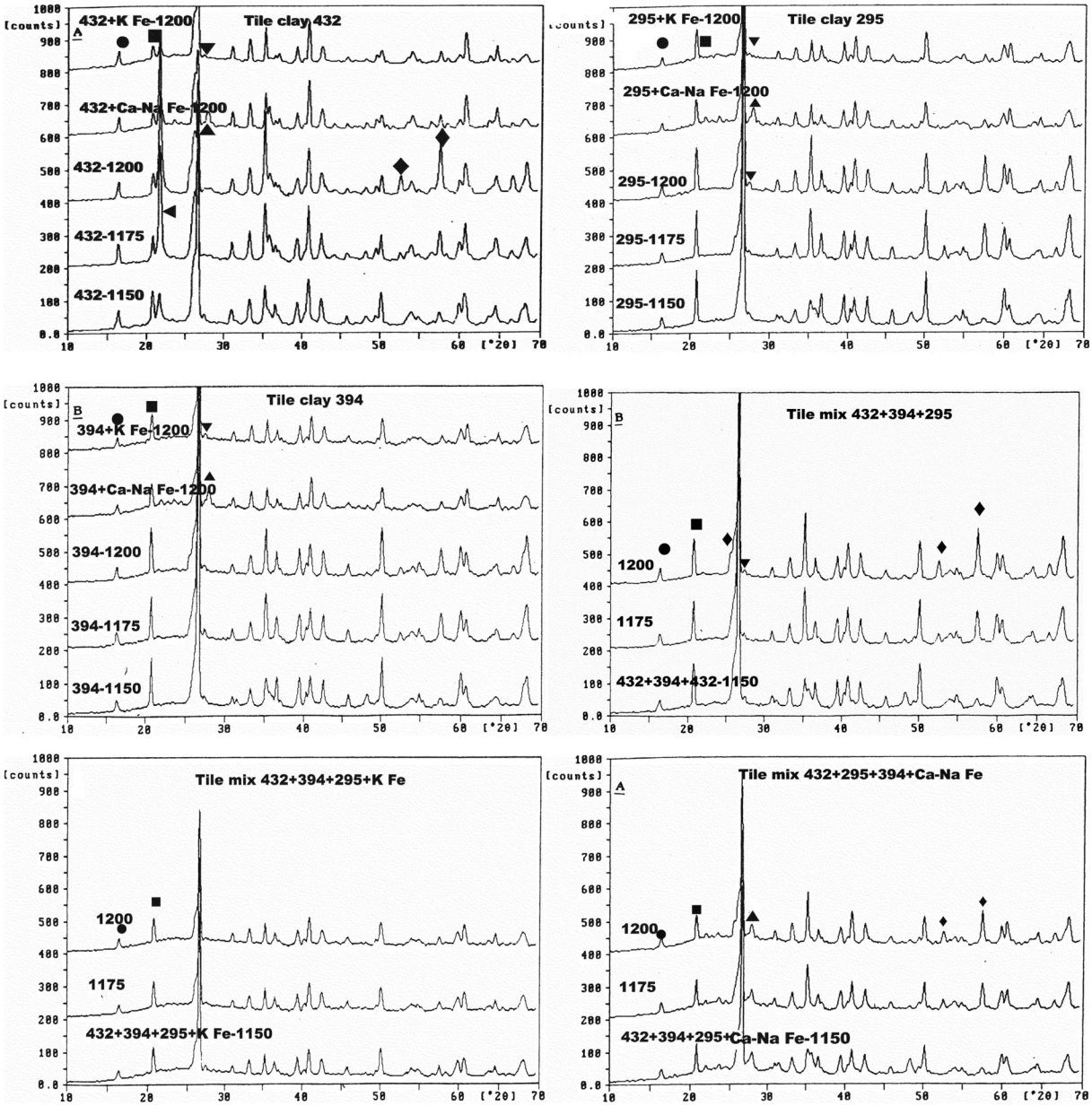

Fig. 2. X-ray diffraction patterns of individual tile clays and their mixture TMIX and TMIX containing 20 wt% K or Ca−Na feldspar (▲: Ca−Na feldspar. ◄: α-cristobalite. ▼: K feldspar ■: Quartz ●: Mullite and ♦: Corundum).

phases were quartz, mullite, and α-cristobalite in the bodies of 432. Three significant changes occurred in the body of 432 during heat treatment. The first change was the appearance of highly intense α-cristobalite which progressively increased with increasing temperature. Secondly, mullite reflections appeared more intense and sharper than those observed in 295 and 394.

In contrast with 394 and 295, no weak feldspar lines were seen at 1150 °C. The α-cristobalite formation is favored in 432 bodies as a result of high kaolinite content and lack of feldspar and illite/mica impurities and having lowest K_2O content (0.74 wt% K_2O) of tile clays. At 1200 °C, the addition of 20 wt% K feldspar inhibited α-cristobalite formation in 432 bodies. However, in the bodies containing 20 wt%Ca-Na feldspar, in contrast to K feldspar, a small amount of cristobalite was identified with 2.51 Å reflection. Although 4.08 Å Ca−Na feldspar and 4.05 Å cristobalite reflections were not observed in the presence of Ca−Na feldspar, because of Ca−Na feldspar, remain still at 1200 °C, and cristobalite reflection 4.05 Å also shift to higher d spacing, when Al^{+3} enters the cristobalite structure.

3.2. QSXRD pattern of tile clay mixture TMIX and TMIX mixed with 20 wt % K feldspar TMIXK and 20 wt% Ca−Na feldspar TMIXC (Fig. 2)

In the TMIX ceramic bodies derived from three tile clays, no α-cristobalite was detected as in individual 295 and 394, and no significant changes were observed in quartz and mullite reflection intensities at 1150 °C. 1175 °C and 1200 °C. Although, the overall K_2O content of tile body mixture (TMIX) is 1,71 wt%, no cristobalite was observed, this high K_2O is enough content to inhibit at 1150–1200 °C, but at over 1200 °C, cristobalite may be formed. The relative intensities of mullite reflections were decreased in TMIXK bodies containing 20 wt % K feldspar when compared to those observed in TMIX without K feldspar. However, in contrast to TMIXK, Ca−Na feldspar reflections remain and may be overlapped with α-cristobalite reflections in TMIXC resulting in difficulties to identify α-cristobalite in the presence of Ca−Na feldspar.

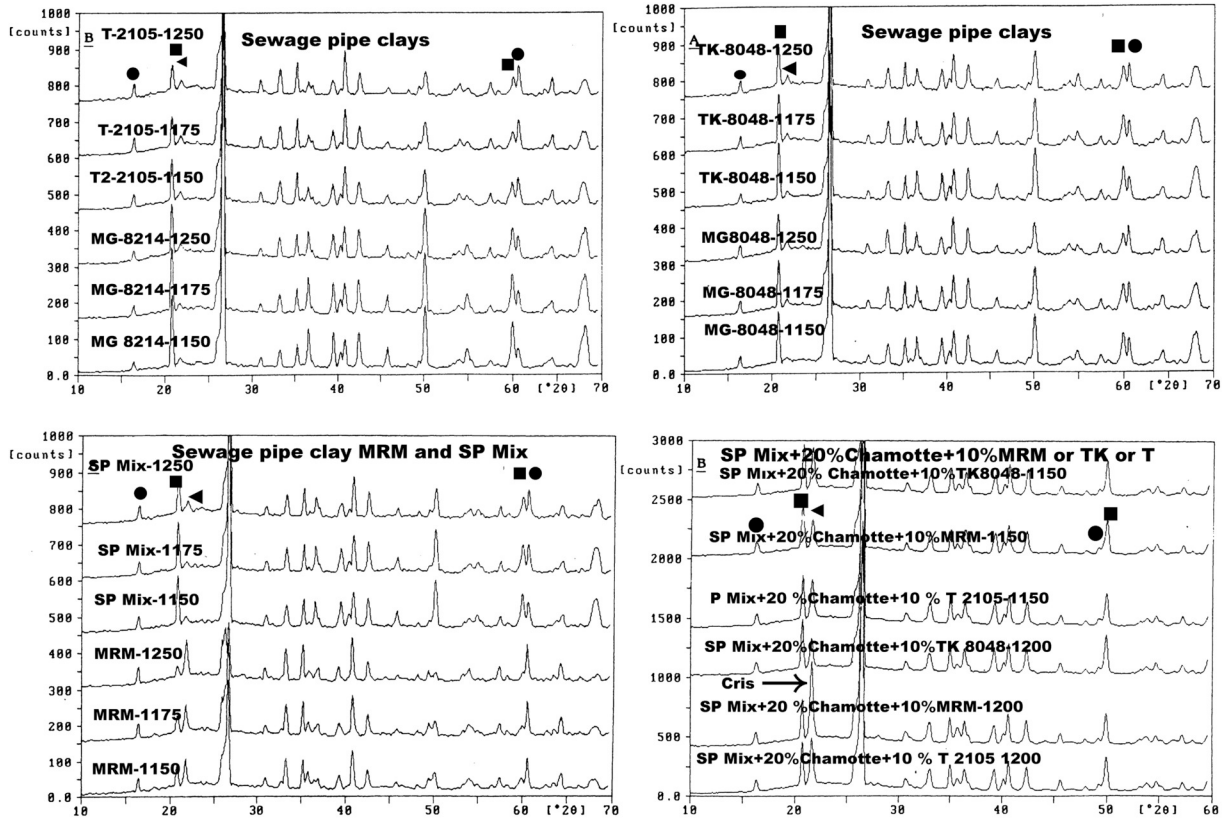

Fig. 3. X-ray diffraction patterns of individual SP clay and their mixtures (◄: α-cristobalite, ■: Quartz, ●: Mullite).

3.3. QSXRD X-ray diffraction patterns of ceramic bodies derived from individual SP clays (MG 8048. TK 8048. MG8214. T2105. MRM) and their mixture SP mix (Fig. 3)

The X-ray patterns of individual raw MG 8048, TK 8048, MG8214, T2105 and MRM clays are shown in Fig. 3. At 1150 °C, 1175 °C and 1250 °C quartz, mullite, and α-cristobalite were detected as major high-temperature phases. The X-ray patterns of ceramic bodies of all SP clays showed similar characteristic lines and intensities except for sample MRM. More α-cristobalite occurs in MRM than those observed in other SP clays because of the presence of high illite/smectite mixed and smectite and Fe minerals and less free quartz content. Addition of 20 wt % MRM caused more α-cristobalite formation in the mixed SP bodies than the bodies derived from other SP body mixtures (Fig. 3).

Observations of SP bodies derived from the SP mixture of three clays (MG8214 + T2105 + MG8048) indicate very weak α-cristobalite reflections for these bodies. However, in the SP mix containing 20 wt% Chamotte + MRM or T2105 or TK048, higher α-cristobalite reflection intensities are observed than those observed in the bodies without chamotte addition and smectitic MRM. The maximum α-cristobalite formation was found in the SP mix bodies containing 20 wt% Chamotte +10 wt% MRM at 1200 °C (Fig. 3).

3.4. QSXRD of ceramic bodies derived from individual Turkish ball clays

3.4.1. DM. KU and ŞE

3.4.1.1. DM (Fig. 4). The major crystalline phases in Raw DM were kaolinite and chalcedony and very low amounts of quartz, whereas, in the ceramic body derived from DM, the phases present at 1000 °C were mullite, α-cristobalite and quartz. The early α-cristobalite formation (980 °C) is attributed to the presence of microcrystalline quartz (i.e., chalcedony). As the temperature increased to 1200 °C, α-cristobalite and mullite reflections intensities also increased. At 1200 °C α-cristobalite diffraction reflections appeared at 21.6 4. 35.626. 44.005 and 56.177 2Θ degrees.

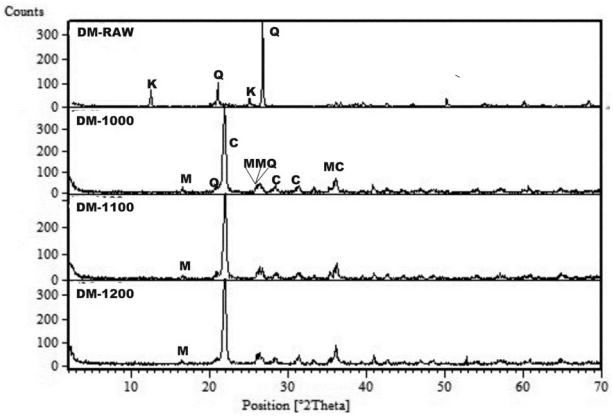

Fig. 4. X-ray diffraction patterns of residual Turkish clay DM fired at 1000 °C, 1100 °C, and 1200 °C.
(K: kaolinite. M: Müllite. Q: Quartz +Chalcedon. C: α-cristobalite)

3.4.1.2. KU (Fig. 5). Opal CT was initially present in raw clay KU. When heated above 1000 °C, the α-cristobalite formation was confirmed by sharpening and an increase in the intensity of 4.04 Å and all other reflections observed at temperatures of 1000 °C and 1100 °C at 1200 °C. Mullite diffraction reflections clearly appear at 2Θ:21.6 4. 35.626. 44.005 and 56.177.

3.4.1.3. ŞE (Fig. 6). In clay ŞE, the major phases found in the raw state were kaolinite and rock crystal quartz. In the ŞE body, in contrast to the DM and KU, α-cristobalite and mullite occurred at 1100 °C similar to WBC HB (kaolinite-rich WBC HB and 432) [14].

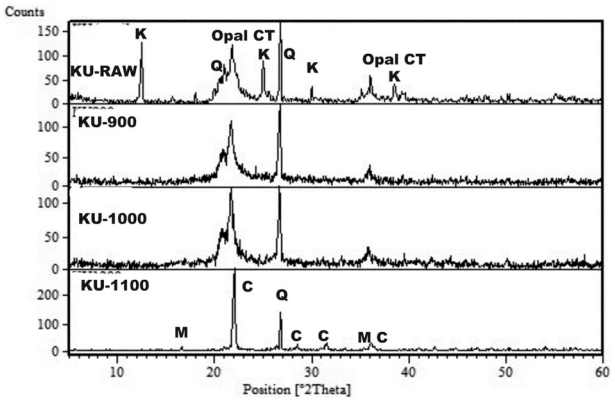

Fig. 5. X-ray diffraction patterns of residual Turkish clay KU fired at 900 °C.1000 °C. and 1100 °C.
(K: kaolinite. M: Müllite. Q: Quartz + Chalcedon. C:α-cristobalite. Opal CT)

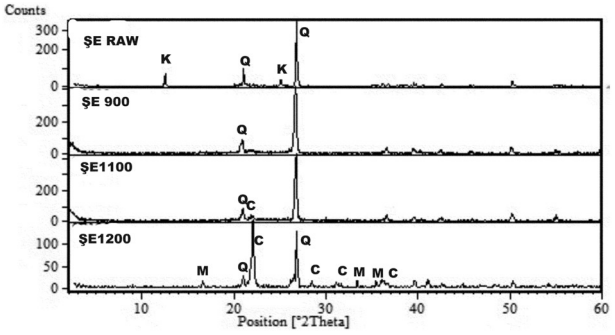

Fig. 6. X-ray diffraction patterns of Turkish ball clay ŞE fired at 1000 °C, 1100 °C, and 1200 °C.
(K: kaolinite. M: Müllite. Q: Quartz + Chalcedony. C: α-cristobalite)

3.5. Scanning electron microscopy

In the photomicrograph depicted in Fig. 7A, the treatment with hot HF produces significantly more solution cavities and pits in amorphous/glassy phase; and both the small rounded and tiny elongated etch pits tended to become greater in size and depth with increasing leaching time. This treatment also resulted in the formation of new cubic shaped and twinned K rich crystalline phases that were precipitated by leaching solutions and were observed on the freshly cracked surface on quartz crystal of Fig. 7B, F (marked with a white arrow). The EDX spectrum of these new crystals displayed strong K and Ca and relatively weak of Si and Al indicating that these aluminosilicates were rich K and Ca. It is widely accepted that dissolution of glasses is incongruent. The chemical composition of new crystals indicates selective leaching of alkali ions from the amorphous/glassy matrix; therefore, leaching also produces a de-alkalized layer. This crystallization confirmed the K rich leaching solution originated from K rich glassy phase but the immediate washing it with water after etching eliminated these new formation crystals as shown. The different crack patterns are severe and numerous around the larger quartz grains as well as within the glassy matrix. In the microphotograph Fig. 7A. It is difficult to differentiate the porosity and the solution pits of the glassy phase. This dissolution pattern shows that the amorphous/glassy phase does not possess a homogeneous composition and structure. The difference between crack patterns of freshly cracked quartz (B) and natural quartz grain surface (C) is easily noticed. The quartz and the freshly cracked surface are seen on the micrographs of Fig. 7B and C. As

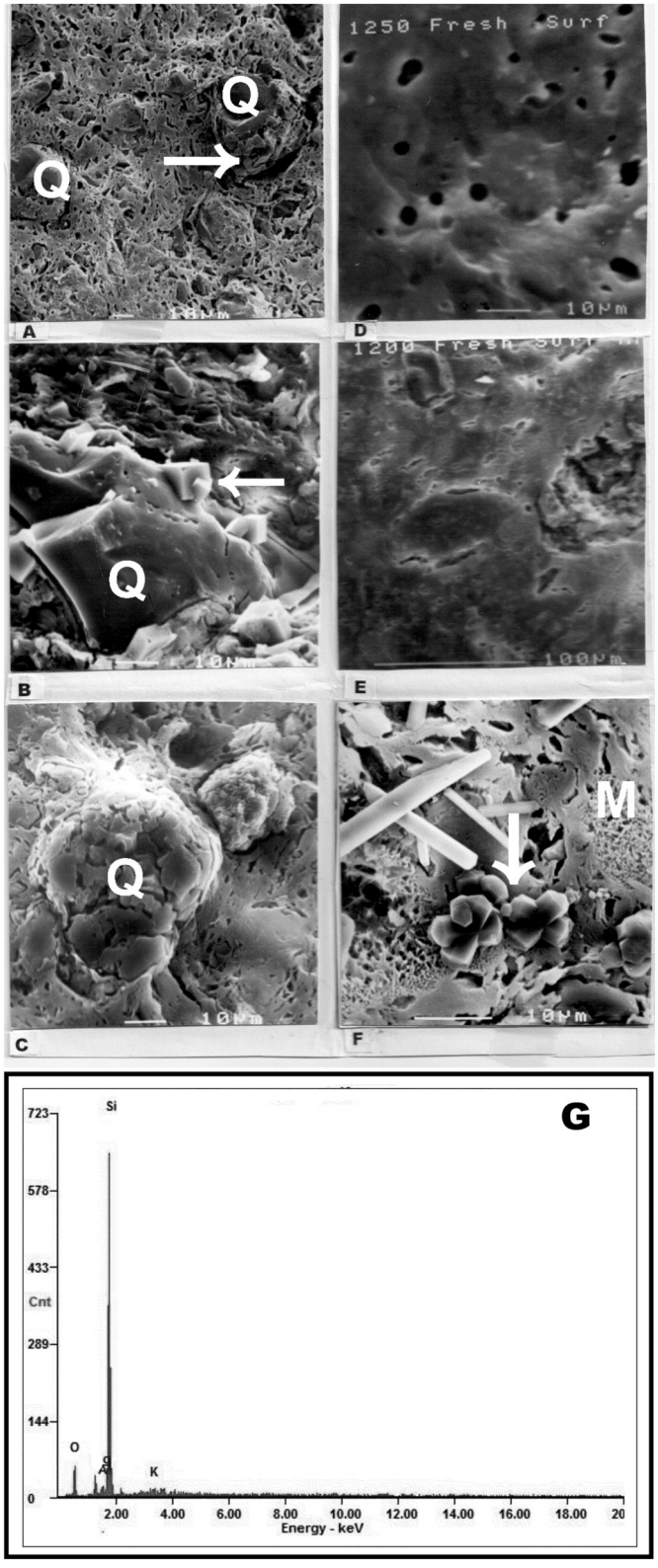

Fig. 7. SEM photomicrographs of fresh fractured and etched surface of TMIXK body (A, B) and cristobalite formation on uncracked surface of quartz (C) the fresh fractured surface of SP Mix (D, E) and K rich crystal precipitated from etching solutions (F) and EDS results of cristobalite formed on uncracked surface of quartz of (G).

Table 5
Measured densities and firing shrinkages of fired tile and SP bodies.

SP bodies	Max F.Tem C°	App den wt %	Real den wt %	Ske Den wt %	Firing shrink wt%	Tile bodies	Max F.Tem C°	App den wt %	Real den wt %	Ske Den wt %	Firing shrink wt%
MG8048	1150	2,25	2,61	2,53	4,22	432	1150	2,26	2,87	2,69	7,39
MG8048	1175	2,30	2,59	2,51	4,68	432	1175	2,30	2,85	2,67	7,52
MG8048	1250	2,33	2,59	2,50	4,47	432	1200	2,30	2,67	2,66	7,86
TK8048	1200	2,23	2,57	2,53	4,14	432 + K Felds	1200	2,36	2,64	2,59	8,01
TK8048	1200	2,30	2,57	2,50	4,60	432 + Ca-Na Felds	1200	2,39	2,59	2,52	7,90
TK8048	1250	2,31	2,55	2,47	4,82	394	1150	2,31	2,82	2,62	7,15
MG8214	1150	2,21	2,60	2,59	3,18	394	1175	2,35	2,81	2,60	7,50
MG8214	1175	2,30	2,60	2,54	4,08	394	1200	2,37	2,64	2,59	7,62
MG8214	1250	2,37	2,55	2,48	4,84	394 + K Felds	1200	2,45	2,59	2,46	7.62.
T2105	1150	2,34	2,55	2,52	5,38	394 + Ca-Na Felds	1200	2,39	2,56	2,48	7,60
T2105	1175	2,42	2,54	2,50	5,50	295	1150	2,31	2,80	2,57	6,54
T2105	1250	2,43	2,54	2,47	4,88	295	1175	2,42	2,74	2,54	6,81
MRM	1150	2,28	2,59	2,43	4,84	295	1200	2,44	2,59	2,54	7,56
MRM	1175	2,24	2,63	2,34	4,42	295 + K Felds	1200	2,46	2,57	2,48	7,20
MRM	1250	1,97	2,61	2,35	3,04	295 + Ca-Na Felds	1200	2,41	2,55	2,46	7,15
SPMIX	1150	2,24	2,61	2,53	3,80	432 + 295 + 394	1150	2,28	2,84	2,64	6,27
SPMIX	1175	2,25	2,60	2,47	3,86	432 + 295 + 394	1175	2,38	2,84	2,61	6,32
SPMIX	1250	2,27	2,60	2,45	4,78	432 + 295 + 394	1200	2,44	2,65	2,61	6,52
SPMIX + CHM + MRM	1100	2,17	2,56	2,53	3.23	432 + 295 + 394 + K Felds	1150	2,30	2,56	2,49	6,52
SPMIX4 + CHM + TK8048	1100	2,24	2,57	2,52	3.12	432 + 295 + 394 + K Felds	1175	2,40	2,56	2,45	6,82
SPMIX + CHM + T2105	1100	2,25	2,58	2,53	3.47	432 + 295 + 394 + K Felds	1200	2,43	2,58	2,47	6,90
SPMIX + CHM + MRM	1200	2,18	2,57	2,54	3.24	432 + 295 + 394 + Ca-Na Felds	1150	2,30	2,76	2,54	5,97
SPMIX4 + CHM + TK8048	1200	2,25	2,57	2,54	3.01	432 + 295 + 394 + Ca-Na Felds	1175	2,42	2,77	2,52	7,22
SPMIX + CHM + 2105	1200	2,24	2,58	2,53	3.10	432 + 295 + 394 + Ca-Na Felds	1200	2,50	2,59	2,52	7,46

CHM = Chamotte. App = Apparent. Max F. Tem = Maximum firing Temperature. SP=SP. SPMIX = 40wt%MG8214 + TK8048 orMG8048 + 10MRM.
True den = Real den, Apparent den = Bulk den, Apparent solid den = Skeletal den, TMIX: 30 wt% 295 + 40 wt% 394 + 30 wt% 432.
TMIXK: 25 wt% 295 + 30 wt% 394 + 25 wt% 432 + 20 wt% K felds TMIXC: 25 wt% 295 + 30 wt% 394 + 25 wt% 432 + 20 wt% Ca–Na felds.
SP Mix: 40 wt% MG 8214 + wt% 40 TK 8048(or MG8048) + 10 wt% T 2105 + 10 wt% MRM.
SP Mix-Chamotte: 80 wt% SP Mix +10 wt% MRM or T2105 or TK 8048 + 20 wt% Chamotte.

shown in the same micrograph of Fig. 7C, the new formation crystobalite on the uncracked surface of quartz confirmed that the curved structure on natural quartz surface is not produced by HF treatment. This curved structure may be indicative of the partial transformation of quartz into α- cristobalite formation (marked with a white arrow in Fig. 7A). As shown in photomicrographs D and E of Fig. 7, relict bubbles (1 μ–2 μ closed porosity) formed in preferred chamotte grain (0.1 mm) and secondary mullite formations and twinned K rich crystal which crystallized from liquid solutions formed after HF leaching was observed in Fig. 7F.

3.6. Evolution of densities, porosities and E moduli of tile and SP bodies

The measured densities and E modulus and calculated porosities of individual tile clays and SP clays and their mixtures with feldspar and chamotte respectively are given in Table 5 and Table 6.

3.7. Densities of tile bodies (Table 5) (Fig. 8)

If the tile clays are arranged by kaolinite content from lower to higher values, the order 295–394-432 is obtained. The density and porosity variation can be observed as a function of the kaolinite content in the same order (Table 5). With increasing kaolinite, apparent densities increase, but real and skeletal densities slightly decrease in all three individual tile clays Fig. 8 Adding 20 wt% both kind of feldspar to individual tile clay increase apparent densities, but decrease drastically real and skeletal densities in these bodies of individual tile clays. On the other hand, in general trend, with increasing temperature, apparent densities increase while real and skeletal densities decrease. With increasing temperature, the same trend is also observed in the bodies derived from a mixture of three tile clays. When pure tile mixture (TMIX) compare with tile mixture containing feldspar, 20 wt% K and Ca–Na feldspar (TMIXK-TMIXC) addition increase the apparent densities but decrease real and skeletal densities with increasing temperature. K feldspar decrease more real and skeletal densities than Ca–Na feldspar.

3.8. Porosities and E modulus of tile bodies

All type of porosities decreases with increasing temperature in all tile bodies derived from pure individual tile clay or their mixture. The addition of 20 wt% K or Ca–Na feldspar to either individual tile clays or the mixture of tile clays results in decreasing of apparent and true porosities, but increase closed porosities. The highest E moduli; 83 GPa and 84 GPa are measured from body derived from TMIXC body containing 20 wt% Ca–Na feldspar and a body derived from 295 tile clay containing 20 wt% K feldspar respectively.

3.9. SP bodies

3.9.1. Densities (Table 5) (Fig. 9)

If the individual SP clays are arranged by kaolinite content from a high value to low, the order MG8048-TK8048-MG8214-MRM –T2105 is obtained. With increasing kaolinite content, the apparent density increases while the skeletal and real density decreases in all bodies derived from individual SP clays (Table 5). With increasing temperature, similar tendencies are observed on the values of all bodies except for MRM. Because MRM contains a considerable amount of smectite and mixed-layer illite/smectite. The apparent and skeletal density sharply decreases with the formation of a black core in MRM bodies as the firing temperature is raised. When SP Mix bodies without chamotte compare with the bodies containing chamotte, no significant changes are observed except for SPMRM body containing smectitic clay and chamotte, with increasing temperature, a slight increase in apparent and real densities is seen. Skeletal and real densities of SPT and SPTK containing 20 wt% chamotte and 10 wt% kaolin and quartz-rich clay, however, slightly decrease and increase are observed in real densities and skeletal densities respectively.

Table 6
Calculated porosities and measured E moduli of fired bodies of tile and SP bodies.

SP Bodies	Max F.Tem °C	App Por. wt %	True Por. wt %	Closed Por. wt%	Elastic mod GPa	Tile bodies	Max F.Tem °C	App Por. wt %	True Por. wt %	Closed Por. wt%	Elastic mod GPa
MG8048	1150	11.07	13.79	2.73	44.66	432	1150	15.99	21.25	5.27	34.00
MG8048	1175	8.37	11.20	2.83	47.32	432	1175	13.86	19.30	5.44	51.00
MG8048	1250	6.80	10.04	3.24	51.34	432	1200	13.53	13.86	0.32	56.00
TK8048	1150	11.86	13.23	1.37	41.06	432 + Ca-Na Felds	1200	8.88	10.61	1.73	63.50
TK8048	1175	8.00	10.51	2.51	48.22	432+ K Felds	1200	5.16	7.72	2.56	74.80
TK8048	1250	6.48	9.41	2.93	51.02	394	1150	11.83	18.09	6.25	39.00
MG8214	1150	14.67	15.00	0.33	28.92	394	1175	9.62	16.37	6.75	46.00
MG8214	1175	9.45	11.54	2.09	33.94	394	1200	8.49	10.23	1.73	61.00
MG8214	1250	4.43	7.05	2.62	54.32	394 + Ca-Na Felds	1200	0.24	5.41	5.16	78.00
T2105	1150	7.14	8.24	1.09	66.06	394 + K Felds	1200	3.63	6.64	3.01	74.00
T2105	1175	3.20	4.72	1.52	61.08	295	1150	10.12	17.50	7.38	47.00
T2105	1250	1.62	4.33	2.71	56.84	295	1175	4.72	11.68	6.95	63.00
MRM	1150	6.17	11.97	5.80	58.40	295	1200	3.94	5.79	1.85	70.00
MRM	1175	4.27	14.83	10.5	54.78	295 + Ca-Na Felds	1200	0.81	4.28	3.47	84.00
MRM	1250	16.17	24.52	8.35	36.42	295 + K Felds	1200	2.03	5.49	3.46	76.00
SPMIX	1150	11.46	14.18	2.71	43.20	432 + 295 + 394	1150	13.64	19.72	6.08	42.00
SPMIX	1175	8.91	13.46	4.55	47.60	432 + 295 + 394	1175	8.81	16.20	7.38	54.00
SPMIX	1250	7.35	12.69	5.35	50.30	432 + 295 + 394	1200	6.51	7.92	1.41	62.00
SPMIX + CHM + MRM	1100	14.23	15.23	1.01	32.30	432 + 295 + 394 + K Felds	1150	7.63	10.16	2.53	63.00
SPMIX4 + CHM + TK8048	1100	14.17	15.18	1.00	33.70	432 + 295 + 394 + K Felds	1175	2.04	6.25	4.21	71.00
SPMIX + CHM + T2105	1100	11.07	12.79	1.72	38.52	432 + 295 + 394 + K Felds	1200	1.62	5.81	4.19	73.00
SPMIX + CHM + MRM	1200	16.11	17.84	1.73	30.00	432 + 295 + 394 + Ca-Na Felds	1150	9.45	16.67	7.22	53.00
SPMIX4 + CHM + TK8048	1200	11.42	12.45	1.03	40.30	432 + 295 + 394 + Ca-Na Felds	1175	3.97	12.64	8.67	73.00
SPMIX + CHM + T2105	1200	11.46	13.18	1.72	44.23	432 + 295 + 394 + Ca-Na Felds	1200	0.79	3.47	2.68	83.00

CHM = Chamotte. App = Apparent. Max F.Tem = Maximum firing Temperature. SP = Sewage pipe.

3.9.2. Porosities and E moduli of SP bodies (Table 6) (Fig. 9)

When individual tile bodies compare with individual SP bodies, one significant change is observed in contrast to tile bodies, and the true and apparent porosities decrease while the closed porosities increase with the increase of firing temperature from 1150 °C to 1250 °C except for MRM body. Increasing of closed porosities may be attributed to high max firing temperature of SP bodies (1250 °C). In tile bodies, apparent, true and closed porosities decrease with increasing temperature from1150°C to 1200 °C. The closed porosity increases at 1175 °C but then decreases at 1200 °C in MRM. In contrast the other individual SP clays, in MRM bodies, the apparent and true porosities increase with increasing temperature. In Table 6 the lower closed porosities calculated from densities of the SP Mix bodies containing 20 wt% chamotte than that of individual SP and SP Mix clays bodies.

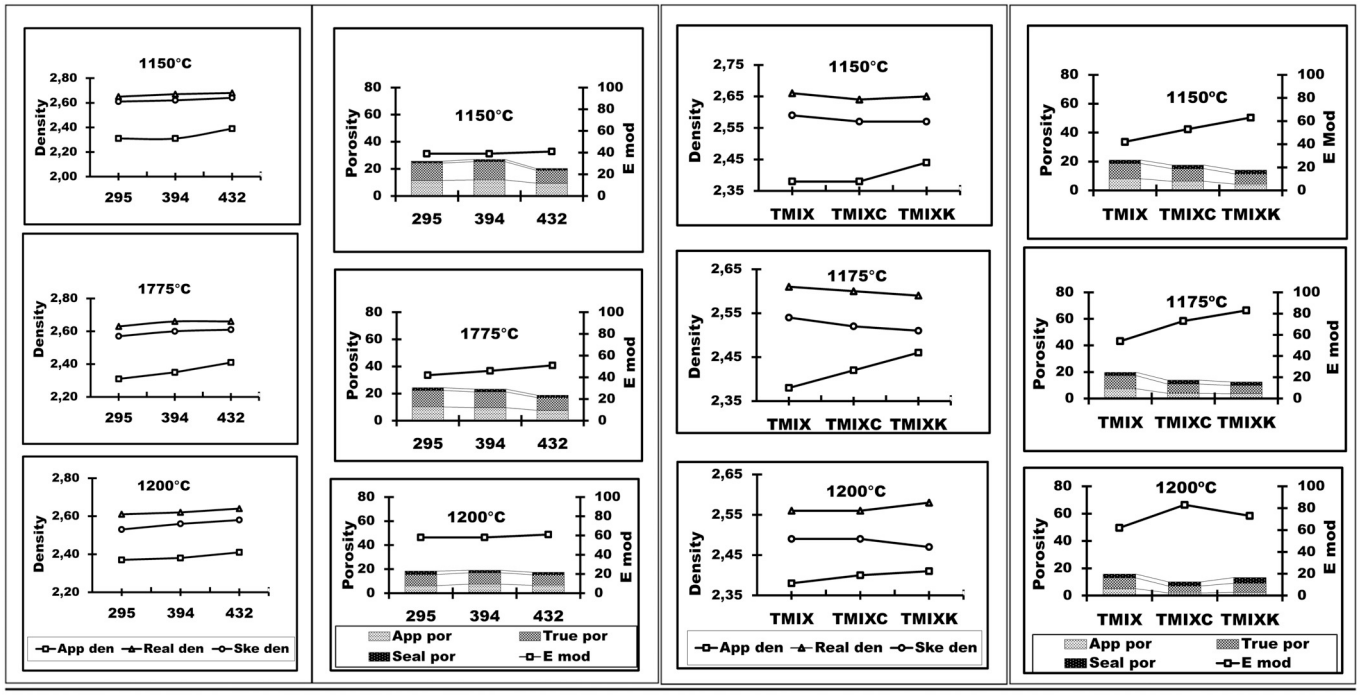

Fig. 8. Evolution of densities, porosities, and E modulus individual tile clays and their mixtures with K and Ca—Na feldspar (TMIXK-TMIXC).

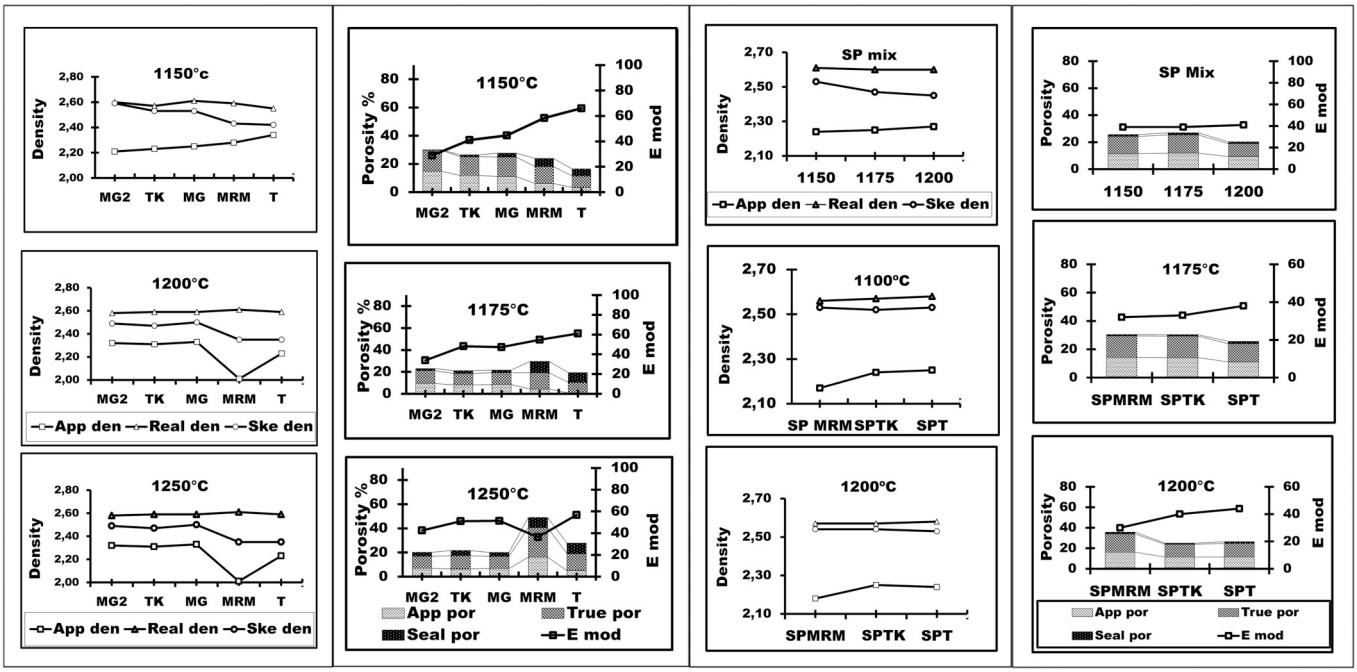

Fig. 9. Evolution of densities, porosities, and E modulus individual tile clay and their mixtures with 20 wt% chamotte (SP Mix, SPMRM, SPTK, and SPT).

3.9.3. Firing shrinkage of tile and SP bodies

The 20 wt% chamotte content in SP Mix reduced shrinkage during firing. Because in the used temperature range 1150–1250 °C, it is supposed that chamotte does not undergo any shrinkage since it was preliminarily fired at the same temperature (SP waste). Chamotte grains behave as inert phases like quartz during sintering, and the large size elongated pores along the chamotte grains whose existence is supposed to be favored by the differential densification during sintering between chamotte grain (0.1 mm) and matrix (Fig. 7d). The chamotte content in the SP Mix is due to the reduced shrinkage during firing from the also higher amount of quartz content of SP clays than those observed of kaolinite-rich tile clays.

4. Discussion

4.1. Background

The former studies by Aras (2004); Aras (2018) laid the groundwork for observing α cristobalite and determining the nature of mullite-α cristobalite formations in ceramic bodies derived from individual WBC. The low crystallinities of kaolinite in WBC minerals resulted in excess spinel formation, and this spinel formation delayed the primary mullite formation as was also observed by Lee et al. (1999). Therefore at 1150 °C α-cristobalite together with the secondary mullite intense reflections were observed in all X-ray patterns of WBC containing low K_2O content such as HB (0.91 wt% K_2O) of Aras (2004) and 432 (0.7 wt % K_2O) clay of this present work. This early cristobalite formation above 1150 °C was also observed in Turkish ball clay ŞE (1 wt% K_2O) in this current study. However, when HB is mixed with 25 wt% illitic KW clay or 20 wt% K feldspar rendering the composition to ~ 2 wt% K_2O ratio and no α-cristobalite formation was observed. An exception occurred with the addition of 20 wt%Ca-Na feldspar which was not sufficient for the inhibition of α-cristobalite formation in HB. In this work, alkaline tile and SP bodies derived from WBC have a high potassium content (maximum-2.47 wt% - minimum-1.79 wt%) which results in a higher occurrence of the amorphous/glassy phase development, thereby retarding the cristobalite and mullite crystallization. In contrast, the individual tile clay body 432 has a considerably lower potassium content (0.74 wt%) and higher cristobalite and mullite. The temperature of cristobalite formations is dependent on wt% K_2O content of liberated silica-rich amorphous/glassy phase. Conversely, Lundin (1964) has concluded through electron microscopy studies of porcelain bodies that the concentration gradients and diffusion rates of K_2O are also the two most important factors affecting mullite and α-cristobalite formations. Antoni et al. (2005) supported the above findings and further found that only the optimal distribution of the potassium ions is provided by using aqueous solution (K_2CO_3) to inhibit α-cristobalite formation in calcined kieselguhr. Li et al. (2009) reported that the α-cristobalite formation detected in the kaolinite included of 3 wt% KNO_3, but no α-cristobalite formation was detected in kaolinite included of 3 wt% K_2SO_4 because KNO_3 and K_2SO_4 contain 1.72 wt% and 1.99 wt% K_2O respectively. This studies by and Li et al. (2009) Antoni et al. (2005) determined and supported the importance of concentration gradients of the critical ~2 wt% K_2O content for the overall chemical composition of green bodies in cristobalite formations. In another work, Önal et al. (2006) claimed that opal CT was mistakenly referred to as α-cristobalite or a mixture of α-cristobalite and tridymite respectively (Güven and Grim, 1972; De Jong et al. 1987; Herdianita et al., 2000; Çolak et al. 2000; Chao and Lu, 2002; Aras, 2004). The study of Aras (2004) does not confirm this claim, where first of all the fired clay is WBC which has no opal CT, and secondly, the heating temperature is 1150 °C which is a sufficiently high temperature for cristobalite formation from the siliceous phase derived from the decomposition of disordered kaolinite of WBC. The heating temperature of smectitic clay and hydrothermal kaolin containing opal CT in the studies of Önal et al., 2006) and Kahraman et al. (2005) is 1050 °C which is also sufficiently high for the transformation of opal CT to α-cristobalite according to Wahl et al. (1961). However, these researchers did not determine cristobalite formations, and their claim above mentioned studies is not true. Moreover, Kahraman et al. (2005) pointed out that the formation temperature of α-cristobalite must be raised over 1713 °C and those α-cristobalite formations above 1050 °C from opal CT and chalcedony seems anomalous because the thermodynamic phase equilibria indicate that cristobalite should be unstable at this higher temperature. However, the metastable phase remains due to the non-equilibrium behavior of α-cristobalite in clay-based ceramic and the

high activation energies required for their transformation to the thermodynamically stable phase. The devitrification of silica glass requires the temperature range of 1200 to 1400 °C to form cristobalite, rather than the more stable phase tridymite. The cristobalite is more open-structured than tridymite and closer in characteristics to the glass phase. Wahl et al. (1961) reported that tridymite was not identified in any fired ceramic bodies and therefore eliminated it as a stable phase in one component silica system of the fired ceramic bodies. Wahl et al. (1961) reported that the non-crystalline amorf silica, chalcedony, opal-CT, chert, and rock crystal quartz transform to α-cristobalite at 900 °C, 950 °C, 1000 °C, 1050 °C, 1050 °C, and 1200 °C respectively. Heating to temperatures above 1000 °C reduces the number of stacking faults, and microcrystalline opals are gradually transformed to more highly ordered forms of α-cristobalite (Jones and Segnit, 1971). Thus, α-cristobalite forms early at ≥1000 °C in DM containing chalcedony and in KU containing opal CT. The diffraction pattern of the cristobalite can be distinguished from that of opal CT by the presence of 2.49 and 2.84 which are absent in opal C and CT and narrow characteristic reflection of 4.04 (FWHM: 0.230–0.287) (Hilier and Lumsdon, 1978; Yılmaz and Kaçmaz, 2012; Elzea et al. 1994). However, in many publications, accurate detection of cristobalite formations from opal CT at ≥1050 °C is often challenging. In one such work. Fuji et al. (1995) reported that the unheated residual KU (Kütahya-Ulaşlar) clay contains a considerable amount of α-cristobalite, but the 4.04 Å reflection of unheated KU has wider FWHM (Fig. 5) than those observed in α–cristobalite in this current study. For this reason, the silica phase of unheated KU is opal CT and transforms to cristobalite at ≥1050 °C (Fig. 5). In the X-ray diffraction pattern of the interrupted quenched samples of KU fired at 900 °C. 1000 °C and 1100 °C the opal CT reflections showed a similar evolution of opal-CT compared with that observed by Elzea et al. (1994).

4.2. Cristobalite sources

The α-cristobalite in clay-based ceramic derived from ball clay originates from two different sources. In the bodies derived from ball clay containing the lower 2 wt% K_2O, the α-cristobalite is primarily formed from liberated silica decomposition of metakaolinite at ≥1100 °C. The little amount of α-cristobalite present may also be transformed from the peripheries of the rock crystal quartz grains by long firing at ≥1200 °C. Tuttle and Cook (1949) confirmed the presence of α-cristobalite by X-ray identifications; Schuller (1963) I used electron microscopy, and Lundin (1964) applied both techniques. The presence of α-cristobalite is also confirmed by characteristic curved structures observed on quartz grain surfaces in micrographs of this current study (Fig. 7 C). The amount of α-cristobalite derived from the transformation of rock crystal quartz increased with rising firing temperatures and with decreasing quartz content. Wahl et al. (1961) observed a gradual increase in the rock crystal quartz intensity (3.34 Å) at approximately 1100 °C but at temperatures above 1100 °C, there is a gradual decrease in quartz intensities and a gradual increase in cristobalite intensities at ≥1200 °C. In addition to the two aforementioned sources of α-cristobalite, the cryptocrystalline silica phases (opaline or chalcedonic silica) is a third source in residual kaolin. The third cristobalite source in residual kaolin is opaline and chalcedonic silica phase. In the literature, for residual kaolin containing no microcrystalline silica phase, i.e., chalcedony or opaline silica and having < 1.5 wt% K_2O content. α-cristobalite formations occur at ≥1200 °C in Zettlist Kaolin of Leonard (1976), English kaolin of Chakraborty (2003) and Kga-1 of Georgia kaolin of Johnson and Pask (1982). Adamo et al. (2013) compared the bodies with equal kaolin/albite ratio, but the different crystallinities (ordered and disordered kaolinite minerals) and reported that more cristobalite formations occur in the bodies containing no albite and disordered kaolin at 1280 °C. These findings support the conclusion that maximum cristobalite occurs in disordered 432 clay of this work and HB clay of Aras (2004) with low K_2O content.

4.3. Densities and E modulus and calculated porosities

In a present study, cristobalite formations and the relevant variations in E modulus and densities of fired tile and SP bodies with elevating temperature were investigated. It is well known that the measurement of E modulus asses is indirectly determining material strength (Allison, 1987; Lee and Yeh, 2008). Here are the results of measured densities and E moduli and calculated porosities as a function of maximum firing temperature, kaolinite, and quartz content, and type of addition (feldspar minerals or chamotte) were discussed. The fired body powder consisting of quartz, mullite and glassy grains each with different densities, hardness, and fineness. These differences (different hardness of glass and crystalline phases) cause the porous glass phase to be more ground than the other crystalline phases (disseminated mullite in the glass facilitates the grinding Fig. 7e) Therefore, the closed porosity embedded in the amorphous/glassy phase is easily destroyed (Fig. 7d). However, the real measured density in this study may be slightly lower than the real values because of the presence of very small pores in the sample (1 μ Fig. 7d). Finally, the microflaws created by different shrinkage and expansion of crystalline and chamotte grain and amorphous/glassy material, the porosity created by the escape of gases, and the relict porosity of the green bodies result in the true(total) porosity of the fired body. The observed size of open pores and closed pores by SEM observations supported this (Fig. 7d, e). SEM observations revealed that there are also three distinct varieties of pores occurrences present in the tile and SP bodies. a) Larger irregular shaped (laminar) voids in the matrix called shrinkage pores (Fig. 7d). They originated from imperfect mixing (segregation of fine kaolinite) and differential consolidation of the fine kaolinitic clay or chamotte grain. Higher porosities of 432 than those of 295 and 394 may be attributed to this type of mechanism. b) Important stress may arise as a result of the α-β quartz and α-β cristobalite inversion or the difference in expansion between the quartz and cristobalite grains and surrounding glassy matrix. This stress also produces three types of cracks within the body; i)-microcracks and flaws within the quartz grains, ii)- pores at the peripheries of the quartz grains, and iii)-cracks throughout the amorphous/glassy matrix. The higher porosities of SP body mixtures containing chamotte and smectitic clays which favors cristobalite formations are attributed above metioned type of mechanism (a and b). The last category porosity observed in SEM is c) Above 1000 °C, bubbling and blistering produce closed pores (1–2 μ) (Fig. 7d,e) in the amorphous/glassy matrix while some open pores also become closed pores. The higher closed porosities of the tile bodies containing feldspar are attributed to the last type “c” type occurrences.

The used Ca—Na feldspar (Na rich-Anorthtite Labradorite-Bytownite) and anorthtite-chamotte of Capoglu and Messer (2004) have different eutectic melting points in tile-body and porcelain-body mixtures respectively. Anorthtite melts at above 1550 °C, but if one alkali is present, at a lower temperature (Tarvornpanich et al., 2008). On the other hand, if newly formed anorthtite formed at quartz and labradorite-bytownite contacts, which was then however melted partly with increasing temperature over 1200 °C when overall wt% Ca content lower than 5 wt% in quartz-rich tile bodies (Dondi et al., 1999). Therefore, Ca—Na feldspar melts more in quartz rick KW than kaolinite-rich HB, and K feldspar melts more in kaolinite-rich HB than quartz-rich KW at 1150–1250 °C, because of the rendering of necessary silica originated from heated kaolinite for ternary eutectic of K feldspar (Aras 2004). When the mineralogical composition of tile and tile clays compared with HB, KW, and HB-KW mixture of Aras 2004 and Aras, 2018, tile clays present similar chemical and mineralogical composition of the 3HB + KW mixture. Therefore, all bodies derived from individual tile clay and 20 wt% Ca- Na feldspar present higher E modulus than that of bodies containing K feldspar except for kaolinite-rich 432 because of different melting behavior as explained above. The measured E modulus level values 83–73 GPa of tile mixture containing Ca—Na feldspar (TMIXC) at 1200 °C which is of similar value to those of measured by

Cavalcante et al. (2004) for tile bodies. According to mechanisms as mentioned earlier, the SP bodies which have lower kaolinite and higher quartz content present lower E moduli than tile bodies. The bodies derived from T 2105 kaolinite richest clay have slightly higher E moduli than the other bodies derived from SP clays. The E modulus of the bodies derived from smectitic MRM clay decrease with increasing temperature. The lowest E moduli of SP body mixtures containing 20 wt % chamotte addition was attributed a high amount of cristobalite formation, and shrinkage cracks around chamotte grain because the second firing of chamotte means that glassy phase of chamotte grain fired again with longer soaking time and cause cristobalite formations. The SP Mix-MRM containing 20 wt% chamotte and 18 wt% MRM (80 wt% SP- Mix +10 wt% MRM + 20 wt% Chamotte) present highest cristobalite formations and lowest E modulus of all studies bodies.

4.4. Mechanism of the strength of clay-based ceramic

By SEM and X-ray analysis, the cristobalite and secondary needle-like mullite were found to yield from liquid phase formed by the transformation of spinel when firing at 1150 °C (Aras 2004; Aras, 2018). Two main factors are affecting the formation of secondary mullite within the fired ball clay; i)- a-poor or disordered kaolinite crystallinity and ii- high content of K containing impurities. The former had a significant effect on the formation of secondary needle-like mullite crystals, constructing the interlocking texture within the glassy phase and the latter decrease the formation temperature of the secondary mullite and cristobalite in WBC. Carty and Senapati (1998) reported that secondary mullite, because of its acicular morphology and smaller needle diameter, might increase strength more than primary mullite. Besides mullite crystal, the presence of cristobalite (cristobalite formed from quartz) instead of quartz in the fired body also produces an increase in strength (Carty and Senapati 1998). This study has reached a somewhat different conclusion from ours; this difference can be explained by different sources of cristobalite of these studies. On the other hand, it is well known that crystalline phase such as mullite tend to increase E modulus, through a predominant mechanism of matrix reinforcement (Mattyasovssky-Zsollnay, 1957; Cavalcante et al. 2004) or dispersion–strengthening (Hasselman and Fulrath, 1966; Warshaw and Seider; Maity and Sarkar, 1996; Carty and Senapati 1998) or mullite hypothesis (Zoellner, 1908; Sane and Cook, 1951). It should be noted that “matrix reinforcement” is widely referenced in many articles as “prestress theory” However, all three main mechanisms in clay-based ceramic should account for strengthing of the clay-based ceramic bodies. Because in tile bodies, the thermal expansion coefficients of the glassy phase don't match of the dispersed secondary mullite crystals which have not only strengthing effect because of “matrix-reinforcement” but also limits the size of the griffits flaws (dispersion strength). Whereas, in a body derived from pure kaolinitic clay body with high strength and E modulus fired at over 1250 °C, the interlocking of growing primary mullite are always formed because of deficiency of enough quartz so that mullite hypothesis may be predominant in this case. In general, in commercial clay-based ceramic bodies with enough amount of glassy phase, both “matrix reinforcement” and “dispersion strength” mechanism should be considered together for the reason of increasing strength and E modulus with increasing mullite content, but the residual quartz plays an opposite role. Besides the crystalline phase dispersed in the glassy phase, porosity also is an important factor on decreasing of strength and E modulus. On the other hand, the strength and E modulus increase with a decrease in either the size of the pore and crystalline grain. The porosity values calculated from density values give only absolute volume percentages of open and closed pores, but changes also take place in the pore and grain size and pore distribution about the firing conditions, mixing degree and type of addition. However, according to Boccaccini and Fan (1997); Rossi (1968), all of mechanism or theory as above mentioned has been neglected in proposed above-mentioned properties (Boccaccini and Fan, 1997; Rossi, 1968).

5. Conclusions

- The results of this work contribute to a better understanding of the effect of an overall K_2O content of a green body on cristobalite formation in fired clay-based ceramic body derived from individual i-ball clay or ii-residual clay or iii- ball clay mixture (tile and SP body mixtures) together with feldspar or chamotte, and smectitic clay.

i. If a body derived from individual ball clay, and its overall K_2O content is lower than 2 wt% K_2O, cristobalite forms from “expulsion” of excess SiO_2 from kaolinite minerals at ≤1100 °C and rock crystal quartz at > 1200 °C, if overall K_2O content higher than 2 wt %, no cristobalite forms.
ii. If a body derived from individual kaolin (residual clay) and or its overall K_2O content is lower than 2 wt% K_2O, cristobalite forms from microcrystalline silica phase; chalcedony or opaline silica cristobalite forms at ≥1000 °C. However, in the case of residual clay containing no microcrystalline silica phase (i.e., Chalcedon) or opaline silica and overall K_2O content of a body is lower than 2 wt% K_2O, cristobalite forms at > 1150 °C, if overall K_2O content higher than 2 wt%, no cristobalite forms.

- In the tile bodies derived from ball clay body mixtures containing K or Ca—Na feldspar (Na rich anorthtite. The K feldspar additions and mica and feldspar impurities rendering ~2 wt% K_2O inhibit α-cristobalite formations. The ~2 wt% K2O content is the threshold value for α-cristobalite formations. However, in Ca—Na feldspar containing bodies, a very small amount of cristobalite was identified with 2.51A reflections.
- Improvement in E moduli of tile bodies containing feldspar was attributed to the secondary mullite present as fracture resistant dispersoids in a viscous glassy matrix. In tile bodies, K feldspar increase E moduli of kaolinite-rich bodies derived from individual tile clays 432 while Ca—Na feldspar increase E modulus in tile bodies derived from 295, 394 and tile body mixtures containing more quartz than individual clay 432.
- The lowest E moduli of SP body mixtures bodies containing 20 wt% chamotte were attributed to high apparent porosity. i.e., large open pores created by high residual quartz, cristobalite and chamotte grains. The results also show that shrinkage decreases with chamotte additions in SP bodies and high shrinkage results into a denser tile body characterized by higher E moduli than those of SP bodies.

Acknowledgements

This study was supported by 2227 Turkey-Tübitak-Hungary -Has European scientific exchange program under the framework of bilateral agreements between The Scientific and Technological Research Council of Turkey) (TUBİTAK) and Hungarian Academy of Science (HAS). The authors would like to express their thanks for financial support provided by TUBITAK and HAS.

References

Adamo, I., Valeria, D., Pavese, A., Vignola, P., Francescon, F., 2013. Na-feldspar (F) and kaolinite (K) system at high temperature: resulting phase composition. Micro-structural features and mullite-glass Gibbs energy of formation, as a function of F/K ratio and kaolinite crystallinity. J. Eur. Ceram. Soc. 33, 3387–3395.
Allison, R.J., 1987. Non-destructive determination of youngs modulus and its relationship with compressive strength, porosity, and density. Geochem. Soc. Spec. Publ. 29, 63–69.
Antoni, D., Russ, W., Pittroff, R.P., Mörtel, H., 2005. Effects of the Fluxing Agents on the Formation of Crystalline Silica Phases during Calcination of Kieselguhr MBAA (Master Brewers Association of the Americas) TQ. vol. 42. pp. 290–296 No. 4.
Aras, A., 2004. The change of phase composition in kaolinite- and illite-rich clay-based

ceramic bodies. Appl. Clay Sci. 24, 257–269.
Aras, A., 2018. The difference between alkaline and alkaline earth effects on high-temperature phase change of clay-based ceramic. Appl. Clay Sci. 164, 2–12.
Aras, A., Albayrak, M., Arıkan, M., Sobolev, K., 2007. Evaluation of selected kaolin clays a raw material for the Turkish cement and concrete industry. Clay Miner. 42, 233–244.
ASTM, E1876-09, 2009. Physical testing standards and mechanical testing standards in Standard Test Method for Dynamic Young'sModulus, Shear Modulus, and Poisson's Ratio by Impulse Excitation of Vibration. ASTM International.
Barbieri, L., Bonfatti, L., Ferrari, A.M., Leonelli, C., Manfredini, T., Settembre Blundo, D., 1995. Relationship between microstructure and mechanical properties in fully vitrified stoneware. In: Vincenzini, P. (Ed.), Ceramics: Charting the Future. vol. 3A. pp. 99–105 Techna Srl. Modena.
Biscaye, P.E., 1965. Mineralogy and sedimentation of recent deep sea clay in the Atlantic Ocean and adjacent seas. Geol. Soc. Am. Bull. 76, 803–832.
Boccaccini, A.R., Fan, Z., 1997. A new approach for the young's modulus-porosity correlation of ceramic materials. Ceram. Int. 23, 239–245.
Capoglu, A., Messer, P.F., 2004. Design and development of a chamotte for use in a low-clay translucent whiteware. J. Eur. Ceram. Soc. 24 (2004), 2067–2072.
Carty, W.M., Senapati, U., 1998. Porcelain raw materials. processing phase evolution and mechanical behavior. J. Am. Ceram. Soc. 81 (1), 3–20.
Cavalcante, T.P., Dondi, M., Ercolani, G., Guarini, G., Melandri, C., Raimondo, M., 2004. The influence of microstructure on the performance of white porcelain stoneware. Ceram. Int. 30, 953–963.
Chakraborty, A.K., 2003. DTA Study of Preheated Kaolinite in the Mullite Formation Region Thermochimica Acta. 398. pp. 203–209.
Chao, C.H., Lu, H.Y., 2002. Stress-induced β→α-cristobalite phase transformation in (Na2O + Al2O3)-codoped silica. Mater. Sci. Eng. A 328, 267–276.
Chavez, L.G., Johns, D.W., 1995. Mineralogical and ceramic properties of refractoryclays from Central Missouri (USA). Appl. Clay Sci. 9, 407–424.
Chmelik, F., Trnik, A., Pesicka, J., Stubna, I., 2011. Creation of microcracks in porcelain during firing. J. Eur. Ceram. Soc. 31, 2205–2209.
Çolak, M., Helvacı, C., Maggetti, M., 2000. Saponite from the Emet Colemanite Mines. Kütahya. Turkey. Clay Clay Miner. 48, 409–423.
De Jong, B.H.W.S., Van Hoek, J., Veeman, W.S., Manson, D.V., 1987. X-ray diffraction and 29 Si magic-angle-spinning NMR of opals incoherent long- and short-range order in opal-CT. Am. Mineral. 72, 1195–1203.
Dondi, M., Guarini, G., Raimondo, M., 1999. Trends in the formation of crystalline and amorphous phases during the firing of clay bricks. Tile Brick. Int. 15 (3), 176–182.
Du, P., Yuan, P., Dong Liu, D., Wang, S., Song, H., Guo, H., 2018. Calcination-induced changes in structure, morphology, and porosity of allophane. Appl. Clay Sci. 158, 211–218.
Dubois, J., Murat Amroune, A., Carbonneau, X., Gardon, R., 1995. High-temperature transformation in kaolinite: the role of the crystallinity and the firing atmosphere. Appl. Clay Sci. 10, 187–198.
Ece, Ö.I., Nakagawa, Z.E., Schroeder, P.A., 2003. Alteration of volcanic rocks and genesis of kaolin deposits in the Şile region, northern İstanbul. Turkey: Clay Mineralogy. Clay Clay Miner. 2003 (51), 675–688.
Elzea, J.M., Odom, I.E., Miles, W.J., 1994. Distinguishing well-ordered opal-CT and opal-C from high-temperature cristobalite by X-ray diffraction. Anal. Chim. Acta 286, 107–116.
Fiederling-Kapteinat, H.G., 2005. The Ukrainian clay mining industry and its effect on the European ceramic raw materials market. Interceram 54, 4–9.
Fuji, N., Kucuksille, N., Yalhı, T., Ozcelik, N., 1980. Some Kaolin Deposits in the West Anatolia Province. MTA. Report No 6818 (in Turkish).
Fuji, N., Kayabalı, İ., Saka, A.H., 1995. Databook of the ceramic raw material of selected areas in Turkey. MTA. Monogr. Ser. 1, 144.
Galos, K., 2011. Influence of mineralogical composition of applied ball clays on properties of porcelain tiles. Ceram. Int. 37 (2011), 851–861.
Garg, N., Skibsted, J., 2014. Thermal activation of a pure montmorillonite clay and its reactivity in cementitious systems. J. Phys. Chem. C 118, 11464–11477. https://doi.org/10.1021/jp502529d.
Glass, H.D., 1954. High-temperature phases from kaolinite and halloysite. Am. Mineral. 39, 193–207.
Gualtieri, A., Bellotto, M., Artioli, G., Clark, M., 1995. Kinetic study of the kaolinite-mullite reaction sequence. Part II: Mullite formation. Phys. Chem. Miner. 22 (4), 215–222.
Guggenheim, S., Bain, D.C., Bergaya, F., Brigatti, M.F., Drits, V.A., Eberl, D.D., Formosa, M.L.L., Galan, M.E., Merriman, R.J., Epicor, D.R., Stanek, H., Watanabe, T., 2001-2002. Report of the Association Internationale Pours l'Etude Des Argiles (AIPEA) Nomenclature Committee: Order. pp. 389–393.
Güven, N., Grim, R.E., 1972. X-ray diffraction and electron optical studies on smectite and α-cristobalite associations. Clay Clay Miner. 20, 89–98.
Hasselman, D.P.H., Fulrath, R.M., 1966. Proposed fracture theory of dispersion-strengthened glass matrix. J. Am. Ceram. Sot. 49, 68–72.
Herdianita, N.R., Rodgers, K.A., Browne, P.R.L., 2000. Routine and ancient silica sinters. Geothermics 29, 65–81.
Herrera, M.S., Hernández, M.F., Cipollone, M., Conconi, M.S., Rendtorff, N.M., 2019. Thermal behavior of samarium oxide –Ball clay mixtures for high macroscopic neutron capture cross section ceramic materials. Appl. Clay Sci. 168, 125–135.
Hilier, S., Lumsdon, D.G., 1978. Distinguishing Opaline Silica From Cristobalite in Bentonites a Practical Procedure and Perspective Based on NaOH Dissolution Clay Minerals. 43. pp. 477–486.
Iqbal, Y., Lee, W.E., 1999. Fired porcelain microstructure revisited. J. Am. Ceram. Soc. 82 (12), 3584–3590.
Johnson, S.M., Pask, J.A., 1982. Role of impurities in the formation of mullite from kaolinite and Al2O3–SiO2 mixtures. Ceram. Bull. 1982 (61), 838–843.
Jones, J.B., Segnit, E.R., 1971. The nature of opal. I. Nomenclature and constituent phases. J. Geol. Soc. Aust. V18, 57–68.
Kahraman, S., Önal, M., Sarıkaya, Y., Bozdoğan, I., 2005. Characterization of silica polymorphs in kaolins by X-ray diffraction before and after phosphoric acid digestion and thermal treatment. Anal. Chim. Acta 552, 201–206.
Keller, W.D., 1968. Flint clays and a flint clay facies. Clay Clay Miner. 16, 113–128.
Kromer, H., 1968–1979. Tertiary Clays in the Westerwald area. Geol. Jb. D. Rhei D Hanover. pp. 69–84 (Ton HB no 105 Ber. dt. keram.Ges., 55. 7) (Ton KW no 56 Ber. dt. keram. Ges. Geol.) (Ton P 161no 75 Ber. dt. keram. Ges).
Kromer, H., 1980. Tertiary clays of Westerwald area Geol. Jb. D. Rhei D Hanover. pp. 69.
Lee, V.G., Yeh, T.H., 2008. Sintering effects on the development of mechanical properties of ired clay ceramics. Mater. Sci. Eng. A 485, 5–13.
Lee, S., Kim, Y.J., Moon, H.S., 1999. Phase transformation sequence from kaolinite to mullite investigated by an energy-filtering transmission electron microscope. J. Am. Ceram. Soc. 82, 2841–2848.
Lemmens, W., 1990. Dynamic Measurements in Materials. American Society for Testing and Materials, Philadelphia.
Leonard, A.J., 1976. Structural analysis of the transition phases in the kaolinite-mullite thermal sequence. J. Am. Ceram. Soc. 60 (1–2), 37–43.
Li, J., Lin, H., Li, J., Wu, J., 2009. Effects of different potassium salts on the formation of mullite as the only crystal phase in kaolinite. J. Eur. Ceram. Soc. 29, 2929–2936.
Lundin, S.T., 1964. Microstructure of Porcelain in Pp 93–106: Microstructure of Ceramic Materials. NBS Mix. Publ, pp. 257.
Maity, S., Sarkar, B.K., 1996. Development of High-Strength Whiteware Bodies. J. Eur.Ceram. Soc. 16, 1083–1088.
Martín-Márquez, J., Ma Rincón, J., Romero, M., 2008. Effect of firing temperature on sintering of porcelain stoneware tiles. Ceram. Int. 34, 1867–1873.
Mattyasovsszky-Zsollnay, L., 1957. Mechanical strength of porcelain. J. Am. Ceram. Soc. 40, 299–306.
Mitchell, D., Vincent, A., 1997. Exploration and appraisal of plastic sedimentary clays for the fine ceramics industry. Appl. Clay Sci. 11 (1997), 311–327.
Okut, M., Gok, S., 1975. Preliminary Report on the Kaolin Deposits at Duvertepe. Sindirgi District. MTA-EHM Open-File Report No. (1975). pp. 1233 (in Turkish).
Okut, M., Demirhan, M., Kose, Z., 1978. Kaolin Deposits in the Emet-Simav District. Kutahya Region. MTA-EHM Open-File Report No. 1233 (in Turkish).
Önal, M., Kahraman, S., Sarıkaya, Y., 2006. Differentiation of α-cristobalite from opals in bentonites from Turkey. Appl. Clay Sci. 35, 25–30.
Onike, F.G.D., Martin, G.D., 1986. Time-temperature transformation curves and the thermal decomposition reactions of kaolinite Mat. Sci. Forum. 7, 73–82.
Pickup, R., 1997. Effect of porosity on Young's modulus of a porcelain. Br. Ceram. Trans. 96, 3.
Rossi, R.C., 1968. Prediction of the elastic moduli of composites. J Am. Cer.Soc. Volume 51 (8), 433–440.
Sane, S.C., Cook, R.L., 1951. Effects of grinding and firing treatment on the crystalline and glass content and physical properties of whiteware bodies. J. Am. Cer. Soc. 34 (5), 145–151.
Schuller, K.H., 1963. Ber. Deut. Keram. Ges. 40, 320 (1964. Trans. Brit Ceram Soc 2. 103).
Slaughter, M., Keller, W.D., 1959. High temperature phases from impure kaolinite. Am. Ceram. Soc. Bull. 38 (12), 702–703.
Stubna, I., Trnık, A., Vozar, L., 2007. Thermomechanical analysis of quartz porcelain in temperature cycles. Ceram. Int. 33, 1287–1291.
Tarvornpanich, T., Souza, G.P., Lee, W.E., 2008. Microstructural evolution in clay-based ceramics I: single components and binary mixtures of clay, flux, and quartz filler. J. Am. Ceram. Soc. 91 (7), 2264–2271.
Thorez, J., 1976. In: Lelote, G. (Ed.), Qualitative Determination of mixed Layers in Practical Identification of Clay Minerals. Liege, Belgium, pp. 42–46.
Trostel, L.J., Wynne, D.J., 1940. Determination of quartz in refractory clays. J. Am. Ceram. Soc. 23–1, 18–22.
Trümer, A., Ludwig, H.M., Schellhorn, M., Diedel, R., 2019. Effect of a calcined Westerwald bentonite as supplementary cementitious material on the long-term performance of concrete. Appl. Clay Sci. 168, 36–42.
Tuttle, M.A., Cook, R.L., 1949. Fundamental study of crystalline and glassy phases in whiteware bodies. J. Am. Ceram. Soc. 32 (9), 279–294.
Vandenberghe, N., 1978. Sedimentology of the Boom Clay (Rupelian) in Belgium, Verhandelingen van de Koninklijke Academie voor Wetenschappen, Letteren en Schone Kunsten van België. (Klasse der Wetenschappen, XL, 147, 137 p).
Wahl, F.M., Grim, R.E., Graf, R.B., 1961. Phase transformations in silica-alumina mixtures as examined by continuous X-ray diffraction. Am. Mineral. 46 (9–10), 1064–1076 1961.
Warshaw, S.I., Seider, R., 1967. Comparison of the strength of triaxial porcelain containing alumina and silica. J. Am. Ceram. Sot. 50, 337–343.
Wilson, I.R., 1998. The constitution. In: Evaluation and Ceramic Properties of Ball Clays Cerâmica. vol.44 (No.287–288 São Paulo May/June/July/Aug).
Yılmaz, H., Kaçmaz, H., 2012. Distinguishing Opaline Silica Polymorphs From -Cristobalite in Gediklerbentonite (Uşak-Türkiye).
Zanelli, C., Raimondo, M., Guarini, G., Dondi, M., 2011. The vitreous phase of porcelain stoneware: composition, evolution during sintering and physical properties. J. Non Cryst. Solids 357, 3251–3260.
Zhou, H.M., Qiao, X.C., Yu, J.G., 2013. Influence of quartz and muscovite on the formation of mullite from kaolinite. Appl. Clay Sci. 80–81 (176-181).
Zoellner, A., 1908. “Zur Frage der Chemischem und Physikalischen Natur der Porzellans” (“some Chemical and Physical Properties of Porcelains”). Sprechsaal 41, 471–473.